Available online at www.sciencedirect.com
SCIENCE DIRECT®
International Journal of Mass Spectrometry 233 (2004) 145–153
International Journal of Mass Spectrometry
www.elsevier.com/locate/ijms

The formation of boron containing fragment ions from the ionization of BCl_3

Natalie A. Love, Stephen D. Price*

Chemistry Department, University College London, 20 Gordon Street, London WC1H 0AJ, UK

Received 1 July 2003; accepted 21 December 2003

Abstract

Relative partial and relative precursor specific partial cross-sections for the electron-impact ionization of BCl_3 have been determined using time-of-flight mass spectrometry and ion–ion coincidence techniques. Data for the formation of B^+, BCl_2^{2+}, BCl^+ and BCl_2^+ relative to BCl_3^+, are reported for ionizing electron energies from 30 to 200 eV.

Keywords: Electronionization; Partial ionization cross-sections; BCl_3; Multiply ionization; Coincidence technique

1. Introduction

Boron trichloride (BCl_3) is widely used in the plasma etching of semiconductors and metals [1–5] and also to dope or deposit boron [6]. A recent report from the National Research Council addressing the "Database Needs for Modeling and Simulation of Plasma Processing" [7] highlighted the lack of reliable partial ionization cross-sections (PICSs) for industrially important molecules such as BCl_3. Accurate values of relevant electron-impact ionization cross-sections are essential for the precise modeling and optimization of plasmas used in industry [8].

Investigations of the electron-impact ionization and photoionization of BCl_3 are limited [9–12]. A recent review of electron interactions with BCl_3 by Christophorou and Olthoff [13] remarks on the lack of data concerning the electron-collision cross-sections with BCl_3 and suggests that further experimental measurements of the total electron-impact ionization cross-section for BCl_3 are needed. An early electron-impact study of the ionization of BCl_3 by Marriot and Craggs, using a Nier 60° mass spectrometer, showed BCl_2^+ to be the most abundant ion formed [9]. More recently, Jiao et al. [10] determined the PICSs of BCl_3 using electron-impact ionization and Fourier transform mass spectrometry, producing absolute PICSs from threshold to 60 eV. To the best of our knowledge, there are no other determinations of the electron-impact ionization cross-sections of BCl_3 in the literature. This lack of data is primarily due to the corrosive and reactive nature of BCl_3, which makes it experimentally challenging to use without severe degradation of the experimental apparatus. The motivation for the current study of BCl_3 is to further investigate the ionization of this highly reactive molecule, over a wider energy range then previous experiments, and to determine the relevant relative PICSs and relative precursor specific PICSs. Relative precursor specific PICSs quantify the contribution from various levels of ionization to the individual product ion yields following an electron–molecule collision. In the current work we are able to distinguish ions formed via single and double ionization.

In the present study a two-dimensional (2D) ion coincidence technique is used to investigate the electron-impact ionization of BCl_3 from 30 to 200 eV. This experimental technique enables the arrival of single product ions, pairs of product ions and, in principle, three product ions at the detector to be identified and quantified. Recent studies using this technique of the ionization of Cl_2 and HCl show the experiment yields accurate relative PICSs over the current ionizing energy range [14,15]. The experiment also allows the contribution to the ion yields from various levels of ionization to be differentiated. In addition, the 2D-ion coincidence technique also provides information on the dissociation

* Corresponding author. Tel.: +44-171-387-7050; fax: +44-171-380-7463.
E-mail address: s.d.price@ucl.ac.uk (S.D. Price).

1387-3806/$ – see front matter © 2004 Elsevier B.V. All rights reserved.
doi:10.1016/j.ijms.2003.12.019

energetics of any multiply charged ions that are formed in the electron–molecule collisions.

2. Experimental

2.1. Experimental apparatus

The apparatus employed in the current investigation is illustrated in Fig. 1 and has been discussed previously in the literature [14,16], so only a brief synopsis is given here. The experiment couples pulsed electron-impact ionization with a time-of-flight mass spectrometer (TOFMS). The arrival times of single ions, pairs of ions and three ions (triples) at the TOFMS's detector, a microchannel plate (MCP), are recorded by the data collection electronics following the repeller plate pulse. This data is used to determine the cross-sections of interest as shown below. The TOFMS used for these experiments is of a standard Wiley–McLaren design [17]. A pulse generator run at 50 kHz controls the pulsing of the electron gun, the pulsing of the repeller plate of the TOFMS and starts the data collection electronics. Following the passage of the pulse of electrons across the source region of the TOFMS, the repeller plate of the mass spectrometer is pulsed from 0 to +400 V. The high electric field this pulse generates in the source region of the TOFMS is sufficient to extract and collect all of the ions in the source region formed with less than 11 eV of translational energy perpendicular to the axis of mass spectrometer. From the source region, the ions are accelerated into a second electric field and then into the field free drift tube. At the end of the drift tube, the ions impinge on the MCP detector. The signals from the MCP are then amplified, discriminated and passed, as "stop" pulses, into a time to digital converter (TDC) which has previously been started by the pulse generator. The resulting ion flight times from the TDC are then transferred to a memory module which, when full, is rapidly dumped to a PC. As discussed in previous publications [14,18], it has been confirmed experimentally that there are no mass discrimination effects occurring in this apparatus, ensuring that quantitative data can be extracted from the mass spectra [19,20].

The apparatus is designed to detect any ions with a translational energy component of less than 11 eV perpendicular to the axis of the mass spectrometer [14]. Curtis and Eland [21] determined the total kinetic energy release (KER) from a dicationic dissociation to commonly be less than 9 eV, so even the most energetic fragment ions formed via dissociative double ionization should reach the detector in our current configuration. The ionic collection efficiency for energetic ions from multiple ionization can in fact be determined from the coincidence data. Hence, even for very highly energetic ions from high levels of ionization, we can in fact assess and allow for any ion losses [14–16,18]. Recent data recorded on our apparatus for the ionization of N_2O [22] is in excellent agreement with the latest reported PICSs [23] for formation of all the fragment ions that are formed. This latest work again indicates that considerable losses of

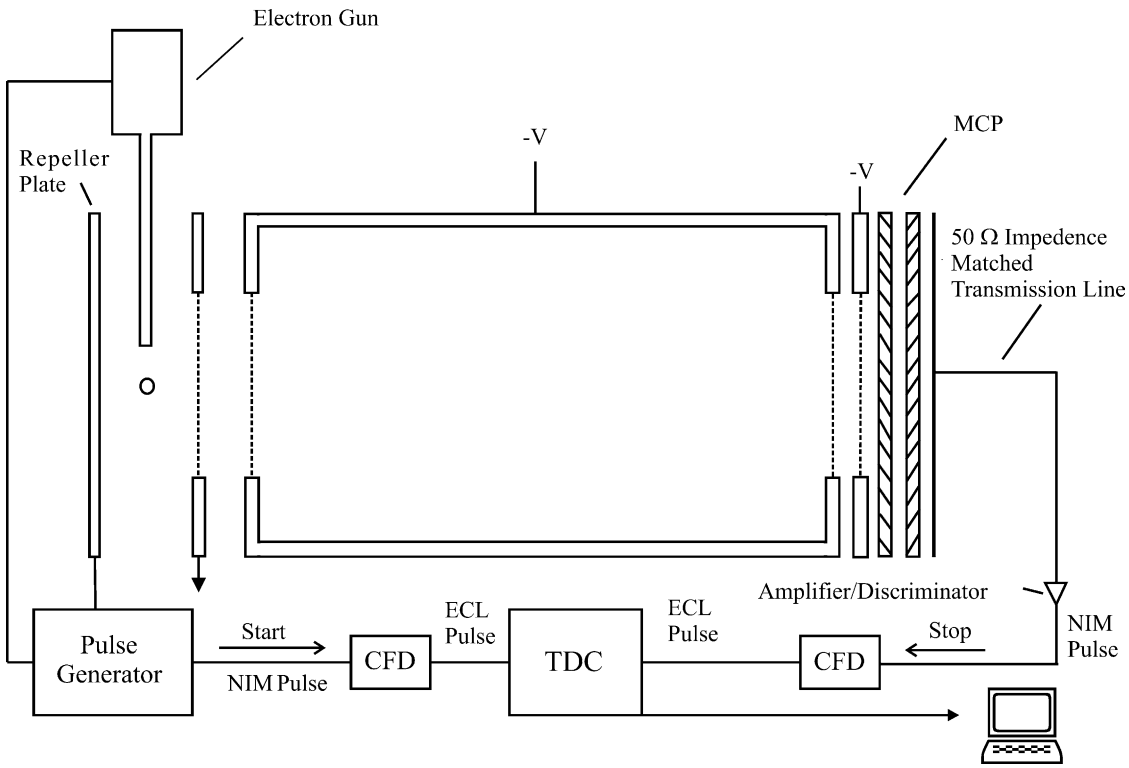

Fig. 1. Schematic diagram of the TOFMS used to study the ionization of BCl_3.

energetic fragment ions occurred in earlier studies of PICSs [24,25].

2.2. Experimental conditions

As discussed in recent publications, the operating conditions we employ involve low electron fluxes and target gas pressures, producing a low ion count rate [14,15,18]. These conditions ensure that there is very much less than one ionization event detected per electron gun pulse. This methodology markedly decreases the likelihood of any accidental coincidences [19,26,27]. Hence, no accidental coincidence subtraction was performed for the spectra reported in this paper, as such contributions to the spectra are minimal.

By operating under these conditions of low pressure and low count rate ions from the background gas in the mass spectrometer can contribute to the mass spectrum. In principle, by recording mass spectra of the empty spectrometer, the contribution of the background gas can be determined and subtracted from each mass spectrum. However, for these experiments using BCl_3, no subtraction is necessary, as the gas signals from the background gas do not overlap with any ion signals from BCl_3.

The corrosive nature of BCl_3 had several detrimental effects on our experiments and on the data they yield. Firstly, exposure to BCl_3 degraded the pulse height distribution from the MCP during each experimental run. To ensure that the ion detection efficiency was constant for each experiment, the MCP was "regenerated" before the next experiment until the mean pulse height from the MCP returned to its original value. This regeneration was achieved by exposing the MCP to air at a pressure of 1×10^{-6} Torr for a period of several hours. The degradation of the MCP also forced us to limit the experimental run times, and reduce to two the number of mass spectra recorded at each electron energy, so that irreversible MCP degradation did not occur. This curtailment of the data acquisition times increases the statistical uncertainty in the cross-sections we report in this paper. Secondly, despite repeated attempts to dry the gas inlet system a white deposit was always observed on the glass. This deposit was also reported by Tokunaga et al. [28] and is attributed to $B(OH)_3$ formation via hydrolysis. Due to this hydrolysis of BCl_3, $H^{35}Cl^+$ and $H^{37}Cl^+$ ion peaks are observed in the mass spectrum. The proximity of these impurity peaks in the mass spectrum to the Cl^+ signals we also observe, and the potential contribution of dissociative ionization of HCl to these Cl^+ signals makes the extraction of reliable data for Cl^+ formation from BCl_3 in our experiments extremely difficult. As a result of these problems, we do not present cross-sections for the formation of Cl^+ from ionization of BCl_3. Tokunaga et al. [28] also report that BCl_3 effectively scavenges O_2 and H_2O, which is confirmed by the observation of trace quantities of $BClOH^+$ in the present experiment and also in the experiments of Jiao et al. [10].

2.3. Data reduction

Events involving a single arrival at the detector following the repeller plate pulse are termed "singles" and the flight times associated with these events are added to a histogram of ion counts against flight time that makes up the mass ("singles") spectrum. The intensities of the peaks in these mass spectra $I[X^+]$ are determined by simply summing the counts in the peak and applying a suitable background correction for the non-zero baseline.

Events involving two ion arrivals at the detector are referred to as "pairs." These events are stored individually and processed off-line. The majority of coincidence signals will consist of two ion arrivals as, over the electron energy range under investigation, the probability of dissociative triple ionization occurring is significantly lower than that of dissociative double ionization. In fact in this study, due to the short run times, no real triple coincidences were detected. Hence, we ignore the contribution of triple ionization to the ion yield in this energy range, as this yield is insignificant at the level of accuracy of our data. As described in other publications [14,15,29,30], the pairs are displayed as a coincidence spectrum: a two-dimensional histogram of t_1 (first ion arrival time) against t_2 (second ion arrival time) for each ion pair. The relative intensities of the peaks in the pairs spectrum can be determined by summing the number of counts within the characteristic 'lozenge' shaped peak [20,30–33]. From the counts in each dissociative channel detected in the coincidence spectrum, appreciating of course that a given product ion can be formed by several channels, we can determine $P[X^+]$, the number of counts in the pairs spectrum for each ion of interest.

The ion intensities recorded in the singles and pairs spectra are processed to yield the relative PICS, $\sigma_r[X^+/BCl_3{}^+]$, and the relative precursor specific PICSs, $\sigma_n[X^+]/\sigma_1[BCl_3{}^+]$. The term precursor specific is used as $\sigma_n[X^+]$ denotes the PICS for forming the X^+ ion from the nth level of ionization, for example $n = 1$ for single ionization. Our data processing algorithm has been described in detail in previous publications [14,15,18], and only a brief description is given here.

The intensity of each singly charged product ion signal in the singles spectrum can be described by Eq. (1), neglecting any contribution from dissociative triple ionization:

$$I[X^+] = f_i N_1[X^+] + f_i(1 - f_i)N_2[X^+] \quad (1)$$

The experimental ion detection efficiency is denoted by f_i and $N_n[X^+]$ represents the number of ionizing events forming X^+, via the loss of n electrons. Hence, the term involving $N_2[X^+]$ in Eq. (1) represents the contribution to the singles spectrum from dissociative double ionization events forming X^+ where the second ion from the dissociation event is not detected. Such ion losses occur, that is $f_i < 1$, because of the 90% transmission of the grids that define the electric fields in the apparatus and the less than unit efficiency of the electronics and detector. So, the intensity of the B^+,

BCl_2^{2+}, BCl^+, BCl_2^+ and BCl_3^+ ions observed in the singles spectra are defined by Eqs. (2)–(6).

$$I[B^+] = f_i N_1[B^+] + f_i(1 - f_i)N_2[B^+] \quad (2)$$

$$I[BCl_2^{2+}] = f_i N_2[BCl_2^{2+}] \quad (3)$$

$$I[BCl^+] = f_i N_1[BCl^+] + f_i(1 - f_i)N_2[BCl^+] \quad (4)$$

$$I[BCl_2^+] = f_i N_1[BCl_2^+] + f_i(1 - f_i)N_2[BCl_2^+] \quad (5)$$

$$I[BCl_3^+] = f_i N_1[BCl_3^+] \quad (6)$$

To determine relative σ_r values, we note that $\sigma_r[X^+/BCl_3^+]$, the relative PIC for formation of a fragment ion X^+ with respect to the parent ion BCl_3^+, is equal to the sum of the cross-sections for forming X^+ via single ionization ($n = 1$) and double ionization ($n = 2$). Specifically where $\sigma[X^+]$ is the PICS for forming X^+ irrespective of the initial level of ionization:

$$\sigma_r\left[\frac{X^+}{BCl_3^+}\right] = \frac{\sigma[X^+]}{\sigma[BCl_3^+]} = \frac{\sigma_1[X^+] + \sigma_2[X^+]}{\sigma_1[BCl_3^+]} \quad (7)$$

Now, under our experimental conditions of low electron flux and ionization rate, $N_n[X^+]$ is proportional to $\sigma_n[X^+]$:

$$\sigma_n[X^+] = kN_n[X^+] \quad (8)$$

where k is a constant for each experiment which is dependent on experimental variables such as the target gas pressure, electron flux across the source region, the duration of the experiment and electron path within the ionization volume [14]. To determine the relative PICSs, the data from the pairs spectra must also be utilized. Our experimental $P[X^+]$ can be written:

$$P[X^+] = f_i^2 N_2[X^+] \quad (9)$$

Hence, we can now express the relative PICSs as:

$$\sigma_r\left[\frac{B^+}{BCl_3^+}\right] = \frac{N_1[B^+] + N_2[B^+]}{N_1[BCl_3^+]} = \frac{I[B^+] + P[B^+]}{I[BCl_3^+]} \quad (10)$$

$$\sigma_r\left[\frac{BCl_2^{2+}}{BCl_3^+}\right] = \frac{N_2[BCl_2^{2+}]}{N_1[BCl_3^+]} = \frac{I[BCl_2^{2+}]}{I[BCl_3^+]} \quad (11)$$

$$\sigma_r\left[\frac{BCl^+}{BCl_3^+}\right] = \frac{N_1[BCl^+] + N_2[BCl^+]}{N_1[BCl_3^+]} = \frac{I[BCl^+] + P[BCl^+]}{I[BCl_3^+]} \quad (12)$$

$$\sigma_r\left[\frac{BCl_2^+}{BCl_3^+}\right] = \frac{N_1[BCl_2^+] + N_2[BCl_2^+]}{N_1[BCl_3^+]} = \frac{I[BCl_2^+] + P[BCl_2^+]}{I[BCl_3^+]} \quad (13)$$

Note that the σ_r values we determine do not depend on f_i. However, if a value of f_i is available then the data analysis can be extended as shown in Eqs. (14)–(20) to determine $\sigma_n[X^+]$ values, quantifying the contributions to each ion yield from single and double ionization. As described in the literature, the ion detection efficiency of our apparatus is determined by recording the singles and pairs spectra following ionization of CF_4 for which accurate relative precursor specific PICSs are available [19,34].

$$\frac{I[B^+] - (1 - f_i)P[B^+]}{I[BCl_3^+]} = \frac{N_1[B^+]}{N_1[BCl_3^+]} = \frac{\sigma_1[B^+]}{\sigma_1[BCl_3^+]} \quad (14)$$

$$\frac{I[BCl_2^{2+}]}{I[BCl_3^+]} = \frac{N_2[BCl_2^{2+}]}{N_1[BCl_3^+]} = \frac{\sigma_2[BCl_2^{2+}]}{\sigma_1[BCl_3^+]} \quad (15)$$

$$\frac{I[BCl^+] - (1 - f_i)P[BCl^+]}{I[BCl_3^+]} = \frac{N_1[BCl^+]}{N_1[BCl_3^+]} = \frac{\sigma_1[BCl^+]}{\sigma_1[BCl_3^+]} \quad (16)$$

$$\frac{I[BCl_2^+] - (1 - f_i)P[BCl_2^+]}{I[BCl_3^+]} = \frac{N_1[BCl_2^+]}{N_1[BCl_3^+]} = \frac{\sigma_1[BCl_2^+]}{\sigma_1[BCl_3^+]} \quad (17)$$

$$\frac{P[B^+]}{I[BCl_3^+]f_i} = \frac{N_2[B^+]}{N_1[BCl_3^+]} = \frac{\sigma_2[B^+]}{\sigma_1[BCl_3^+]} \quad (18)$$

$$\frac{P[BCl^+]}{I[BCl_3^+]f_i} = \frac{N_2[BCl^+]}{N_1[BCl_3^+]} = \frac{\sigma_2[BCl^+]}{\sigma_1[BCl_3^+]} \quad (19)$$

$$\frac{P[BCl_2^+]}{I[BCl_3^+]f_i} = \frac{N_2[BCl_2^+]}{N_1[BCl_3^+]} = \frac{\sigma_2[BCl_2^+]}{\sigma_1[BCl_3^+]} \quad (20)$$

Having explained above the details of the data reduction, in the discussion of the data below we abbreviate the relative PICS and relative precursor PICSs to $\sigma_r[X^+]$, $\sigma_1[X^+]$ and $\sigma_2[X^+]$, where $\sigma_r[X^+/BCl_3^+] = \sigma_r[X^+]$, $\sigma_1[X^+]/\sigma_1[BCl_3^+] = \sigma_1[X^+]$ and $\sigma_2[X^+]/\sigma_1[BCl_3^+] = \sigma_2[X^+]$.

3. Results

Mass and coincidence spectra were recorded at ionizing electron energies between 30 and 200 eV. These data were analyzed as described above to derive the relative PICSs and precursor specific relative PICSs. These derived cross-sections are shown in Figs. 2–5, and are listed in Table 1, as a function of electron energy. The points shown in Figs. 2–5 represent the average of the two data values and the bars extend between the two values. This representation provides a clear view of the data scatter. The data scatter is significantly larger than in our previous work because only two determinations are averaged to give the final value, as opposed to 5 or more in work with less corrosive gases [14,15,18]. Note that $\sigma_r[BCl_2^{2+}] = \sigma_2[BCl_2^{2+}]$ and that the BCl_2^+ ion is the most abundant ion formed following

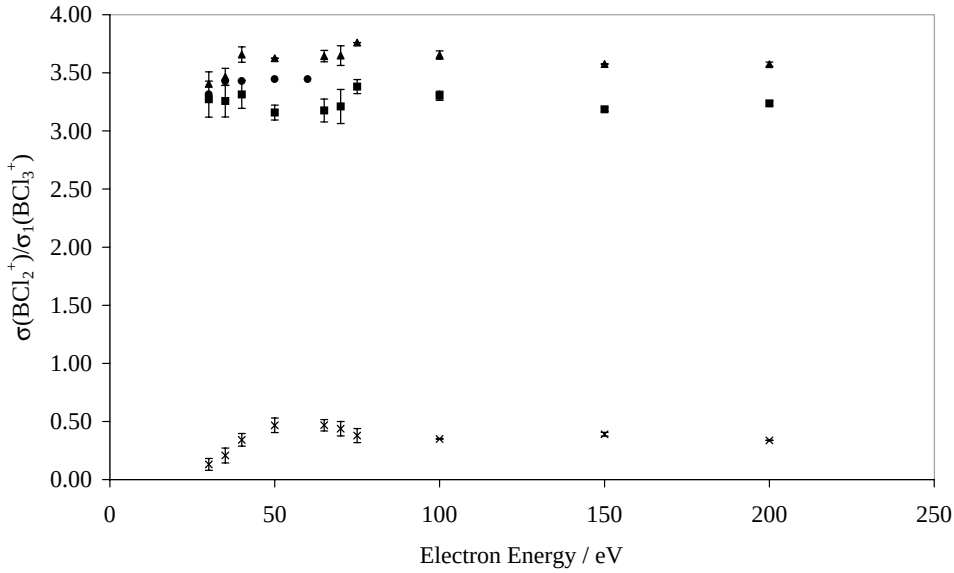

Fig. 2. The relative PICS and precursor specific PICSs determined for forming BCl_2^+ following electron-impact ionization of BCl_3. The $\sigma_r[BCl_2^+]$ values are marked with ▲, $\sigma_1[BCl_2^+]$ with ■ and $\sigma_2[BCl_2^+]$ with ×. The markers show the average of two experimental determinations and the bar shown represents how far each data point lies from the average value. Data are expressed relative to the formation of BCl_3^+. Comparison is made with relative partial cross-sections derived from the absolute PICSs of Jiao et al. [10] (●).

electron-impact ionization of BCl_3 at all the electron energies we investigated. Data are presented for the formation of B^+, BCl_2^{2+}, BCl^+, BCl_2^+ and BCl_3^+. As described above, we do not report cross-sections for the formation of Cl^+.

To derive the $\sigma_n[X^+]$ values we determined a value of f_i, as described in previous publications [14,15], by simultaneously recording singles and pairs spectra following ionization of CF_4, as the relevant ionization cross-sections are well determined for this molecule [19,34]. This procedure resulted in an average value of f_i of 0.12 ± 0.01. This value of f_i is lower than our previous determinations [14,18]. We believe this low value of f_i is principally due to MCP degradation during preliminary experiments with BCl_3. As described above, to ensure that f_i remains constant for each experiment the pulse height distribution was monitored after every experiment and the MCP regenerated if necessary.

The pairs spectra we record following ionization of BCl_3 exhibit four primary dissociation channels: $B^+ + Cl^+$, $Cl^+ + Cl^+$, $BCl^+ + Cl^+$, $BCl_2^+ + Cl^+$. At 200 eV the relative intensities of these channels are 1:0.70:0.60:0.71. However, in the one long data collection run we performed, for 8000 s at 200 eV electron energy, where the counting statistics are superior to the "short" duration spectra we normally recorded

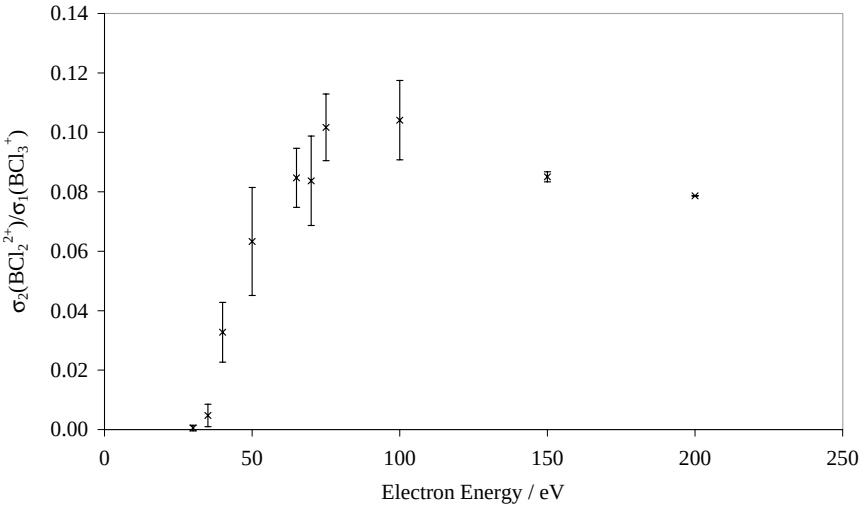

Fig. 3. The relative PICS for forming BCl_2^{2+} ($\sigma_r[BCl_2^{2+}]$) by electron-impact ionization. See Fig. 2 for details.

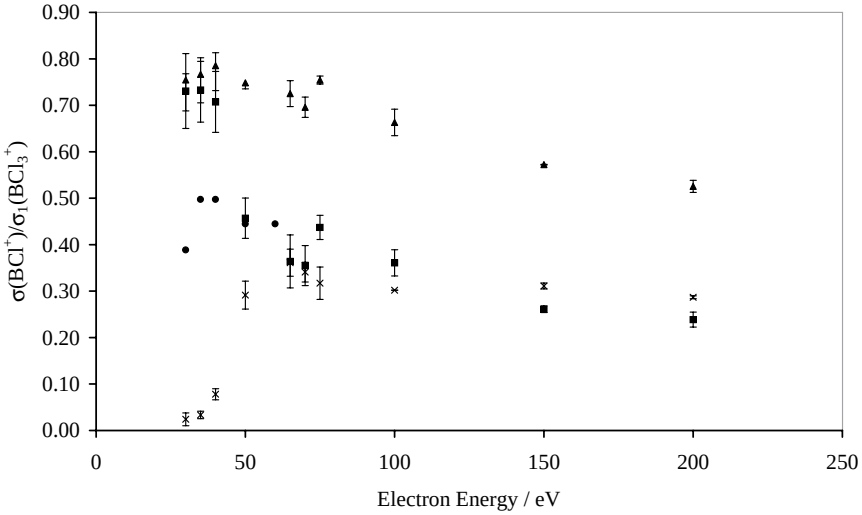

Fig. 4. The relative PICS and precursor specific PICSs determined for forming BCl^+ following electron-impact ionization of BCl_3. The $\sigma_r[BCl^+]$ values are marked with ▲ $\sigma_1[BCl^+]$ with ■ and $\sigma_2[BCl^+]$ with ×. Comparison is made with relative partial cross-sections derived from the absolute PICSs of Jiao et al. [10] (●). See caption for Fig. 2 for details.

Table 1
Relative precursor specific PICSs and relative PICSs for the formation of the indicated product ion from BCl_3 as a function of incident electron energy.

Energy (eV)	$\sigma_1[B^+]/\sigma_1[BCl_3^+]$	$\sigma_2[B^+]/\sigma_1[BCl_3^+]$	$\sigma_r[B^+]/\sigma_1[BCl_3^+]$	$\sigma_2[BCl_2^{2+}]/\sigma_1[BCl_3^+]$	$\sigma_1[BCl^+]/\sigma_1[BCl_3^+]$
200	0.72(2)	0.45(1)	1.17(1)	0.08(1)	0.46(2)
150	0.80(3)	0.50(1)	1.30(3)	0.09(1)	0.50(1)
100	0.99(10)	0.50(2)	1.48(12)	0.10(2)	0.59(4)
75	1.18(5)	0.47(6)	1.65(1)	0.10(1)	0.68(1)
70	0.92(14)	0.46(2)	1.38(16)	0.08(2)	0.62(4)
65	0.90(14)	0.39(1)	1.29(15)	0.08(1)	0.64(5)
50	0.95(7)	0.25(21)	1.20(28)	0.06(3)	0.68(3)
40	1.01(21)	0.04(1)	1.05(22)	0.03(1)	0.77(8)
35	0.79(15)	0.03(1)	0.82(14)	0.00(1)	0.76(9)
30	0.60(30)	0.01(1)	0.61(29)	0.00(1)	0.75(10)
	$\sigma_2[BCl^+]/\sigma_1[BCl_3^+]$	$\sigma_r[BCl^+]/\sigma_1[BCl_3^+]$	$\sigma_1[BCl_2^+]/\sigma_1[BCl_3^+]$	$\sigma_2[BCl_2^+]/\sigma_1[BCl_3^+]$	$\sigma_r[BCl_2^+]/\sigma_1[BCl_3^+]$
200	0.29(1)	0.75(2)	3.50(3)	0.34(1)	3.84(2)
150	0.31(1)	0.81(1)	3.49(1)	0.39(2)	3.88(2)
100	0.30(1)	0.90(4)	3.57(5)	0.35(1)	3.92(5)
75	0.32(5)	1.00(5)	3.67(2)	0.38(9)	4.05(7)
70	0.34(3)	0.96(1)	3.55(14)	0.44(9)	3.99(5)
65	0.36(4)	1.00(1)	3.54(9)	0.47(7)	4.01(2)
50	0.29(4)	0.97(1)	3.52(2)	0.47(9)	3.99(7)
40	0.08(2)	0.85(6)	3.58(11)	0.34(8)	3.92(3)
35	0.03(1)	0.79(8)	3.42(12)	0.21(9)	3.63(3)
30	0.02(2)	0.77(8)	3.38(16)	0.13(7)	3.51(9)

The values represent the average of two determinations. The numbers in parentheses indicate the difference between the average value and actual data points in the last figure of each cross-section.

to avoid MCP degradation, we also see traces of a $BCl^+ + Cl_2^+$ dissociation channel.

The presence of boron (^{10}B, ^{11}B) and chlorine (^{35}Cl, ^{37}Cl) isotopes means that at least four ion pair peaks are detected for each dissociation channel except $Cl^+ + Cl^+$. However, these isotopic peaks are not fully resolved in the pairs spectrum making any extraction of isotopic specific cross-sections impossible. Hence, we sum all the isotopic data to give cross-sections for the individual product ions.

4. Discussion

In this section, we will discuss the data we derive concerning the formation of B^+, BCl_2^{2+}, BCl^+, BCl_2^+ and BCl_3^+ (Figs. 2–5, Table 1).

4.1. BCl_2^+ and BCl_2^{2+} formation

The values of $\sigma_r[BCl_2^+]$ we determine are in good agreement with the values derived from the absolute PICS

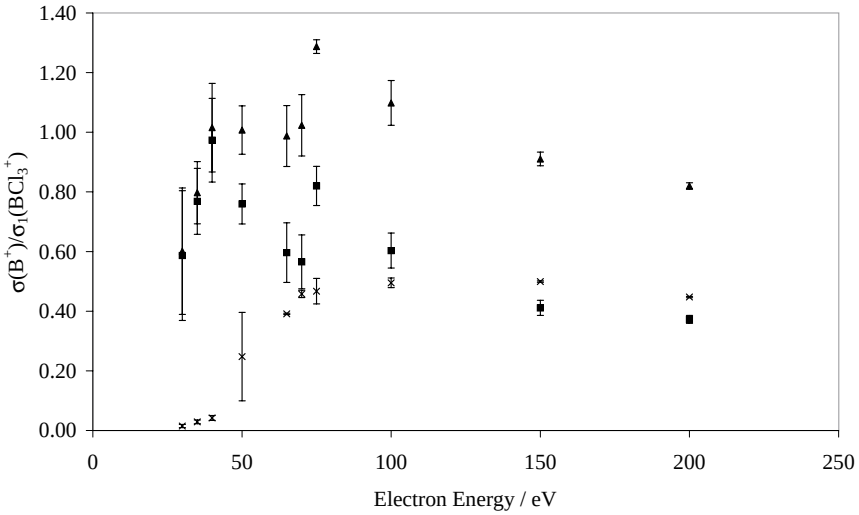

Fig. 5. The relative PICS and precursor specific PICSs determined for forming B^+ following electron-impact ionization of BCl_3. The $\sigma_r[B^+]$ values are marked with ▲, $\sigma_1[B^+]$ with ■ and $\sigma_2[B^+]$ with ×. See Fig. 2 for details.

recently presented by Jiao et al. [10] (Fig. 2). This agreement clearly indicates that, in our experiments, no BCl_2 is produced by the reaction of BCl_3 on the surfaces of the spectrometer or the filament. If significant surface formation of BCl_2 were occurring, the BCl_2 would then be ionized, causing the $\sigma_r[BCl_2{}^+]$ values to be larger than the data of Jiao et al. [10] which is not the case. This conclusion, that no neutral BCl_2 is generated from reactions of BCl_3 in the spectrometer, is important in the data interpretation below.

We observe $BCl_2{}^{2+}$ in the mass spectrum in low abundance. As shown above, since we know there is no dissociation of BCl_3 to form BCl_2 in our apparatus, then these $BCl_2{}^{2+}$ ions must come from dissociative double ionization of BCl_3. At 100 eV, the relative PICS for $BCl_2{}^{2+}$ is 3% of the $BCl_2{}^+$ relative PICS. The appearance potential for $BCl_2{}^{2+}$ is determined to be 31.5 ± 2.0 eV (Fig. 3). This value is derived by applying a weighted least squares fit to the relative PICS at electron energies from 30 to 50 eV, using a suitable background correction to allow for the proximity of the $BCl_2{}^{2+}$ ion peak to adjacent signals in the mass spectrum. This simple technique, which is appropriate for our electron energy resolution and sampling interval, has been shown to yield estimates of appearance potentials in good agreement with more accurate methods of threshold determination [14,15]. In 1957, Marriot and Craggs [9] determined the threshold for $BCl_2{}^{2+}$ to be 33.77 ± 0.07 eV and our appearance energy estimate for $BCl_2{}^{2+}$ is in good agreement with this value. The $BCl_2{}^{2+}$ dication was not detected by Jiao et al. [10]. However, $\sigma_r[BCl_2{}^{2+}]$ is 0.063 at 50 eV, which places the PICS for the formation of $BCl_2{}^{2+}$ close to lowest values reported by Jiao et al. [10]. Hence, it is possible that $BCl_2{}^{2+}$ is not detectable at an electron energy of 50 eV in their experiments or decays over the significant time needed to record a FT mass spectrum.

4.2. BCl^+ formation

Fig. 4 illustrates that below 65 eV the $\sigma_r[BCl^+]$ values we derive from our data are 50% larger than those derived from the cross-section determinations of Jiao et al. [10]. However, the general form of the energy dependence, decreasing with increasing electron energy, is similar for the two sets of results. One possible reason for the discrepancy is a difference in efficiency of energetic ion collection between our experiment and the FTMS apparatus used by Jiao et al. [10]. If BCl^+ ions are formed with a significant kinetic energy they may not be efficiently retained and detected in the FTMS employed by Jiao et al. [10] which requires significant ion residence times. Unfortunately, Jiao et al. [10] do not detail the detection efficiency of their apparatus for translationally "hot" ions. It is well established [21,23,31,35–37] that dissociative multiple ionization is a common source of energetic monocations and double ionization may well account for some of the difference between the relative PICSs derived from the data of Jiao et al. [10] and the data presented here. However, Fig. 4 clearly shows the contribution of dissociative double ionization to the BCl^+ yield is low between 30 and 40 eV, and thus it seems that in this energy region single ionization must contribute significantly to the yield of energetic BCl^+ ions missed by Jiao et al. [10]. At 50 and 60 eV where the contribution of double ionization (∼40%, Fig. 4) to the yield of BCl^+ is now significant (Fig. 4) the data of Jiao et al. [10] still lie close to our values of $\sigma_1[BCl^+]$ implicating single ionization in the production of energetic BCl^+ ions. The formation of highly translationally energetic ions from single and double ionization is well established [38,39] and we feel that the loss of such ions in the FTMS experiments of Jiao et al. [10] is the most probable explanation of the differences between their results and ours. Indeed, to support that conclusion, as discussed below,

we have definitive evidence for the formation of energetic B^+ ions from the dissociative double ionization of BCl_3, yet Jiao et al. [10] report no B^+ ions are formed.

Of course, an alternative explanation for the disagreement between the $\sigma_r[BCl^+]$ values we derive from our data and those derived from the data of Jiao et al. [10] is that the BCl_3 neutral is reacting within our spectrometer to produce neutral BCl which is subsequently ionized. Such a possibility is hard to eliminate completely. However, as noted above, we see no evidence for the dissociation of BCl_3 to BCl_2 in our experiments or have ever had evidence for the dissociation of other reactive molecules in previous experiments [14,15,18]. In addition, the BCl^+ we detect from double ionization is formed together with a Cl^+ ion and hence, given the definitive absence of degradation of BCl_3 to BCl_2 in the apparatus, must arise from double ionization of BCl_3. Clearly, further investigations are needed to definitively resolve the source of the discrepancy between our data and that of Jiao et al. [10] for the formation of BCl^+.

4.3. B^+ formation

The observation of significant quantities of the B^+ ion in our singles and pairs spectra again does not correspond with the data of Jiao et al. [10], where no B^+ ions were detected (Fig. 5). Again, as discussed above, the origin of this discrepancy could be inefficient collection of energetic B^+ ions in the experiments of Jiao et al. [10], or breakdown of BCl_3 to boron atoms, which are subsequently ionized in our apparatus. However, as shown below, we have clear evidence that energetic B^+ ions from double ionization, which we see clearly in our pairs spectra, certainly arise from the dissociation of doubly ionized BCl_3. Indeed our data show that $\sigma_2[B^+]$ constitutes more than 30% of $\sigma_r[B^+]$ above 100 eV. Our data also show that these energetic B^+ ions are present at electron energies as low as 50 eV (Fig. 5), where no B^+ ions are reported by Jiao et al. [10]. Hence, we feel again the loss of energetic ions in the experiment of Jiao et al. [10] is again the most likely source of the difference between their results and ours. Of course, some contribution to our values of $\sigma_1[B^+]$ from decomposition of BCl_3 to boron atoms, which are then ionized, cannot be ruled out. However, the definitive detection of B^+ ions from the double ionization of BCl_3 provided by our pairs spectra certainly means that energetic ions are not efficiently detected in the experiments of Jiao et al. [10] and it is thus possible energetic B^+ ions from the dissociation of BCl_3^+, which may contribute significantly to our $\sigma_1[B^+]$ values, are also not detected.

4.4. Dissociative double ionization

As mentioned above, the pairs spectra we record following ionization of BCl_3 exhibit four different decay channels: $B^+ + Cl^+$, $Cl^+ + Cl^+$, $BCl^+ + Cl^+$, $BCl_2^+ + Cl^+$. We recorded one pairs spectrum for sufficient duration to achieve good enough statistics to investigate the mechanism of formation for the $B^+ + Cl^+$ ion pair, which accounts for 35% of the total dication dissociations detected. As has been described before in the literature, the gradient of the coincidence peak in the "pairs spectrum," a 2D histogram of intensity of the pairs signal as a function of the flight times of the two ions, can provide an insight into the mechanism of the charge-separating dissociation [29,30]. This insight is possible as the gradient of the peak reflects the correlation between the momenta of the two fragment ions. For the dominant isotopes, the gradient of the $B^+ + Cl^+$ coincidence peak is determined to be -0.45 ± 0.05. Immediately, this gradient tells us that ion pair does not originate from a simple two body dissociation of BCl^{2+}, which would give a peak with a gradient of -1, as the momenta of the Cl^+ and B^+ would have to be equal and opposite. A dissociation pathway that would generate a coincidence peak with the observed gradient is a sequential reaction mechanism with initial charge separation:

$$BCl_3^{2+} \rightarrow BCl^+ + Cl_2^+ \quad (21)$$

$$\downarrow \qquad \downarrow$$

$$B^+ + Cl + Cl^+ + Cl \quad (22)$$

This fragmentation pathway should result in a coincidence peak with a gradient of -0.48, in excellent agreement with the experimental value. Further support for this dissociation pathway comes from the observation of weak signals corresponding to the fragmentation of BCl_3^{2+} to BCl^+ and Cl_2^+ in the long duration spectrum we recorded at 200 eV, the first step in the proposed route for the formation of B^+ and Cl^+.

Considering the other dicationic dissociation channels we observe, the $BCl_2^+ + Cl^+$ ion pair can only originate from direct dissociation of BCl_3^{2+}. The $BCl^+ + Cl^+$ ion peak appears to have a gradient of approximately -1, suggesting either a three-body direct dissociation from BCl_3^{2+}, or, perhaps more probably since we detect long-lived BCl_2^{2+} ions, the two-body dissociation of BCl_2^{2+} formed in an initial neutral-loss step from BCl_3^{2+}. The mechanism for forming the $Cl^+ + Cl^+$ ion pair cannot be determined from our data due to the 'dead time' in the pairs spectra where $t_1 = t_2$, due to the discriminator. This dead time means we miss a significant fraction of the $Cl^+ + Cl^+$ coincidences, which we can correct for numerically, but makes determining the peak gradient with any accuracy impossible. We have considered the possibility that the $Cl^+ + Cl^+$ signal originates from dissociative double ionization of any traces of Cl_2 present in the sample. However, the Cl_2^+ signal in the singles spectrum is only just above our detection limit and much of this signal must result from the dicationic dissociation to $BCl^+ + Cl_2^+$. However, if we assume all of the Cl_2^+ signal in the mass spectrum is from ionization of Cl_2, then the relevant precursor specific ionization cross-sections [14] indicate that only 4% of the detected $Cl^+ + Cl^+$ coincidences could originate from dissociative double ionization of Cl_2, at 200 eV. Hence, we conclude the $Cl^+ + Cl^+$ coincidences must come

predominantly from ionization of BCl_3, as they cannot originate from ionization of BCl and we have determined above that there is no ionization of neutral BCl_2 occurring in our apparatus.

5. Conclusions

Using pulsed electron-impact ionization, coupled with time-of-flight mass spectrometry, we have determined the relative partial and relative precursor specific PICSs for the formation of B^+, BCl_2^{2+}, BCl^+ and BCl_2^+ relative to BCl_3^+ from 30 to 200 eV. To the best of our knowledge, this is the first time that relative precursor specific PICSs have been derived for BCl_3. Comparison between our data and the only other quantitative study of the electron-impact ionization of BCl_3 has been made. Agreement with this earlier work is excellent for the formation of BCl_2^+, however some inconsistencies exist for the formation of BCl^+ and B^+. These inconsistencies may be accounted for by the earlier experiments failing to detect all the energetic fragment ions.

Acknowledgements

The authors acknowledge helpful discussions with Tilmann Märk and Paul Scheier regarding the collection of energetic ions in experiments determining partial ionization cross-sections. In addition, the authors would like to acknowledge an EPSRC studentship for NAL, a Leverhulme Trust Research Fellowship for SDP and the support of the MCInet [RTN1-2000-00027] European network.

References

[1] M.W. Cole, G.F. McLane, D.W. Eckart, M. Meyyappan, Scanning 15 (1993) 225.
[2] S.J. Pearton, W.S. Hobson, C.R. Abernathy, F. Ren, T.R. Fullowan, A. Katz, A.P. Perley, Plasma Chem. Plasma Process. 13 (1993) 311.
[3] A.T. Demos, H.S. Fogler, J. Fournier, M.E. Elta, AICHE J. 41 (1995) 658.
[4] J.W. Lee, J. Hong, E.S. Lambers, C.R. Abernathy, S.J. Pearton, W.S. Hobson, F. Ren, Plasma Chem. Plasma Process. 17 (1997) 155.
[5] K.J. Nordheden, X.D. Hua, Y.S. Lee, L.W. Yang, D.C. Streit, H.C. Yen, J. Vac. Sci. Technol. B 17 (1999) 138.
[6] A. Slaoui, F. Foulon, C. Fuchs, E. Fogarassy, P. Siffert, Appl. Phys. A Mater. Sci. Process. 50 (1990) 317.
[7] Database needs for modeling and simulation of plasma processing. National Research Council (National Academy Press), Washington, 1996.
[8] L.G. Christophorou, J.K. Olthoff, J. Phys. Chem. Ref. Data 27 (1998) 1.
[9] J. Marriot, J.D. Craggs, J. Electron. Control. 3 (1957) 194.
[10] C.Q. Jiao, R. Nagpal, P. Haaland, Chem. Phys. Lett. 265 (1997) 239.
[11] V.H. Dibeler, J.A. Walker, Inorg. Chem. 8 (1969) 50.
[12] H. Biehl, K.J. Boyle, D.M. Smith, R.P. Tuckett, K.R. Yoxall, K. Codling, P.A. Hatherly, M. Stankiewicz, J. Chem. Soc. Faraday Trans. 92 (1996) 185.
[13] L.G. Christophorou, J.K. Olthoff, J. Phys. Chem. Ref. Data 31 (2002) 971.
[14] P. Calandra, C.S.S. O'Connor, S.D. Price, J. Chem. Phys. 112 (2000) 10821.
[15] S. Harper, P. Calandra, S.D. Price, Phys. Chem. Chem. Phys. 3 (2001) 741.
[16] C.S.S. O'Connor, N. Tafadar, S.D. Price, J. Chem. Soc. Faraday Trans. 94 (1998) 1797.
[17] W.C. Wiley, I.H. McLaren, Rev. Sci. Instrum. 26 (1955) 1150.
[18] C.S.S. O'Connor, S.D. Price, Int. J. Mass Spectrom. 184 (1999) 11.
[19] M.R. Bruce, C. Ma, R.A. Bonham, Chem. Phys. Lett. 190 (1992) 285.
[20] M.R. Bruce, L. Mi, C.R. Sporleder, R.A. Bonham, J. Phys. B At. Mol. Opt. Phys. 27 (1994) 5773.
[21] D.M. Curtis, J.H.D. Eland, Int. J. Mass Spectrom. Ion Process. 63 (1985) 241.
[22] N.A. Love, S.D. Price, J. Chem. Phys. (in preparation).
[23] B.G. Lindsay, R. Rejoub, R.F. Stebbings, J. Chem. Phys. 118 (2003) 5894.
[24] J. Lopez, V. Tarnovsky, M. Gutkin, K. Becker, Int. J. Mass Spectrom. 225 (2003) 25.
[25] I. Iga, M. Rao, S.K. Srivastava, J. Geophys. Res. Planets 101 (1996) 9261.
[26] D.A. Hagan, J.H.D. Eland, Org. Mass Spectrom. 27 (1992) 855.
[27] L.J. Frasinski, M. Stankiewicz, P.A. Hatherly, K. Codling, Meas. Sci. Technol. 3 (1992) 1188.
[28] K. Tokunaga, F.C. Redeker, D.A. Danner, D.W. Hess, J. Electrochem. Soc. 128 (1981) 851.
[29] J.H.D. Eland, F.S. Wort, R.N. Royds, J. Electron. Spec. Relat. Phenom. 41 (1986) 297.
[30] J.H.D. Eland, Mol. Phys. 61 (1987) 725.
[31] S. Hsieh, J.H.D. Eland, J. Phys. B At. Mol. Opt. Phys. 30 (1997) 4515.
[32] L.J. Frasinski, A.J. Giles, P.A. Hatherly, J.H. Posthumus, M.R. Thompson, K. Codling, J. Electron. Spec. Relat. Phenom. 79 (1996) 367.
[33] P. Jukes, A. Buxey, A.B. Jones, A.J. Stace, J. Chem. Phys. 109 (1998) 5803.
[34] M.R. Bruce, R.A. Bonham, Int. J. Mass Spectrom. Ion Process. 123 (1993) 97.
[35] M. Lundqvist, D. Edvardsson, P. Baltzer, M. Larsson, B. Wannberg, J. Phys. B At. Mol. Opt. Phys. 29 (1996) 499.
[36] M. Lundqvist, D. Edvardsson, P. Baltzer, B. Wannberg, J. Phys. B At. Mol. Opt. Phys. 29 (1996) 1489.
[37] D. Edvardsson, M. Lundqvist, P. Baltzer, B. Wannberg, S. Lunell, Chem. Phys. Lett. 256 (1996) 341.
[38] D. Rapp, P. Englander-Golden, D.D. Briglia, J. Chem. Phys. 42 (1965) 4081.
[39] J.H.D. Eland, Photoelectron Spectroscopy, 2nd ed., Butterworths, 1984, p. 212.